Journal of Alloys and Compounds 925 (2022) 166729

Contents lists available at ScienceDirect

Journal of Alloys and Compounds

journal homepage: www.elsevier.com/locate/jalcom

Investigating the impact of growth time of CdSe quantum dots on the structure and optical properties of its nanocomposites with SiO_2 for improvement of optical devices

Ahmed I. Abdel-Salam[a], A. Khalid[b], M.M. Awad[c], Yasmein Hussein[d], R.M. Ahmed[e,*]

[a] Nanotechnology Research Center (NTRC), The British University in Egypt (BUE), Suez Desert Road, P.O. Box 43, El-Shorouk City, Cairo 11837, Egypt
[b] Department of Basic Engineering Sciences, Faculty of Engineering (Shoubra), Benha University, Benha, Egypt
[c] Physics Department, Loughborough University, Loughborough, Leicestershire LE11 3TU, UK
[d] Faculty of Nanotechnology of Postgraduate Studies, Cairo University, Egypt
[e] Physics Department, Faculty of Science, Zagazig University, 44519 Zagazig, Egypt

ARTICLE INFO

Article history:
Received 2 June 2022
Received in revised form 2 August 2022
Accepted 8 August 2022
Available online 10 August 2022

Keywords:
$CdSe-SiO_2$ nanocomposite
VELF
Optical properties
TEM
XRD
FTIR

ABSTRACT

This study effectively succeeded in synthesizing CdSe QDs and CdSe- SiO_2 nanocomposites with controllable tunable size and spectacular morphology by using a solvothermal technique. UV–visible spectroscopy was used to study the effect of the growth time of CdSe QDs on the optical properties of its nanocomposite with SiO_2. The structure of the prepared nanocomposites of CdSe- SiO_2 was studied through the measurements of X-ray diffraction (XRD), transmission electron microscopy (TEM), and Fourier transform infrared spectroscopy FTIR. The Effective Mass Approximation model (EMA), Simple Exponential Function (SEF), and Polynomial Fitting Functions (PFF) were employed to compute nanoparticle sizes, providing particle sizes of 3.86, 4.19, and 3.72 nm, respectively, for CdSe- SiO_2 nanocomposites (2 min). For the same nanocomposite, these theoretical values were comparable to the experimental values of the particle sizes deduced from measurements of TEM (4.5 nm) and XRD (3.4 nm). The deduced optical parameters of CdSe-SiO_2 nanocomposite, such as refractive index, dielectric constant, optical conductivity, electrical susceptibility, and some others, relied on the growth time of CdSe QDs. The absorption peaks of CdSe -SiO_2 nanocomposites suffered from a bathochromic shift which increases as the growth time of CdSe QDs increases. Increasing the growth time of CdSe QDs resulted in increasing the reflection loss factor and decreasing the optical electronegativity. The values of the volume energy loss function (VELF) are greater than the values of the surface energy loss function (SELF) for the different nanocomposites. Consequently, the fast electrons miss their energies through their propagation within the studied materials more than through traveling on their surfaces. The enhancement of n values of nanocomposites of CdSe-SiO_2 by increasing the growth time can candidate them to be usefully applied as antireflection coating for solar cells.

1. Introduction

Nanotechnology, which has greatly contributed to the advancement of innovative technical horizons, is currently the most important factor in the development of modern society [1–9]. Quantum dots (QDs) are considered a fascinating family of semiconductor nanostructures with diameters ranging from 1 to 10 nanometers. They have overcome global stagnation by making substantial advances in numerous technology areas [10,11]. According to fundamental physics, QDs are comparable to semiconductor bulk materials. Therefore, they are regarded as an ideal model system for understanding the molecular tuning of material properties during phase transition [12]. In point of fact, the optical and electrical properties of QDs can be adjusted through modification of their size and form [13–16]. As a result, QDs have become widely used in a variety of applications, including optoelectronic devices, optical data storage, optical data communication, solar cells, laser quantum dots, catalysts, photo-catalysts, biological labeling, etc. [12,17]. Due to its high exciton-Bohr radius and its area of optics, Cadmium Selenide (CdSe QD) is the most widely used semiconductor quantum dots (QDs) for optical applications [18].

* Corresponding author.
E-mail address: rania.7.8.2016@gmail.com (R.M. Ahmed).

https://doi.org/10.1016/j.jallcom.2022.166729
0925-8388/

Silica is a type of metal oxide defined by its low crystallization temperature and low free-energy landscape, both of which are a result of its very flexible siloxane linkages. Such low crystallization heat makes silica the best glass former agent [19]. Silica exists in numerous forms, such as fumed and amphidromous. The most abundant inorganic component of the earth's crust is crystalline quartz silica [20], which is structured in a tetrahedral shape [SiO_4]. At high temperatures, however, silica is organized in hexagonal 6-membered rings through siloxane bonds connecting two silicon centers [21]. Through a pH-dependent condensation process, amorphous silica nanoparticles, microparticles, and macroparticles have been generated under the biosphere [22]. The SiO_2 nanoparticles have many advantages, including enhanced mechanical properties, a large surface area, and low toxicity. Therefore, it can be employed in various industrial applications such as thermoplastic polymers and electronic packing [23–25]. The contained nanopore structures of silica NPs can be hybridized with other materials to generate promising functional nanocomposite materials. Because of their significant antireflective properties, surface coatings made of SiO_2 NPS could be used in a variety of applications, including solar cell and solar heater surfaces that require lower surface reflection. This could be accomplished by fabricating an antireflective SiO_2 NPS film that improves light transmittance [26,27].

Furthermore, SiO_2 can improve the colloidal stability of the QDs in polar liquids at different conditions of pH and ionic strength. In extremely oxidative conditions such as water, the characteristics of semiconductor QDs can rapidly degrade, resulting in substantial loss of their optical properties, specifically the drop in their photoluminescence quantum yield (PLQY). T. Aubert et al. solved these issues by encapsulating CdSe/CdS QDs in silica NPs via a water-in-oil microemulsion technique, resulting in a composite with excellent physicochemical stability and PLQY [28]. Moreover, the dye-sensitized solar cell (DSSC) has greater performance and photo-conversion efficiency (PCE) than quantum dots-sensitized solar cells (QDSSC), which might be related to QDSSCs' interfacial recombination [29–31]. As a result, several attempts have been made to increase the QDSSC performance by passivating the QDs surfaces. The passive layer, which may be constructed of SiO_2 [32], Al_2O_3 [33], or ZrO_2 [34], might prevent electrons from transferring from the photoanode to holes in the electrolyte and act as a blocking layer [35]. Liu, J., et al. developed CdS/CdSe QDs with double passivation using ZnS/SiO_2 to be used as co-sensitizer in the QDSSC, demonstrating that the double passivation with ZnS/SiO_2 improves the PCE by about 55% compared to the QDSSC without passivation [35]. Ning Liu, et al. [36] succeeded in creating nanocomposite of SiO_2-coated CdTe/CdSe QDs by hybridizing silica with Cd derivatives QDs. It has been investigated that the decoration of SiO_2 with CdS [37] and CdSe [38] give highly reactive photocatalyst nanohybrid composites with enhanced optical parameters [39,40], including linear and nonlinear optical parameters [40–44]. Also, an improvement in the nonlinear refractive index of the prepared nanocomposite of CdO–SiO_2 was recorded by Badran et al. [45].

In this regard, the creation of silica-modified optoelectronic materials is the most recent research focus. This study included discussing the effect of the growth time of CdSe QD on the optical parameters of nanocomposites of CdSe-SiO_2. Among the optical parameters that have been computed are relaxation time, optical mobility, optical resistivity, Wemple-Didomenico oscillating parameters, group velocity dispersion, and others. This study extended to estimate the particle size theoretically by using some models. The obtained theoretical values of particle size were compared with the experimental values deduced from XRD and TEM analysis. FTIR was an effective tool for understanding the structure of the produced nanocomposites.

2. Experimental work

2.1. Materials

No further purification of the used chemical compounds was required. The studied samples were prepared by using cadmium oxide (CdO, Fluka, 99.99%), silica powder (SiO_2, Merck 99.9995%), powder of selenium (Se, Strem 99%), TriOctylPhosphine oxide (TOPO, Fluka 97%), Oleylamine (O.Am, Sigma Aldrich 70%), Trioctylphosphine (TOP, Sigma Aldrich, 90%) and Oleic Acid (Merck 99%).

2.2. Synthesis of CdSe-SiO_2 nanocomposite

CdSe-SiO_2 nanocomposites were synthesized using the hot injection method, as previously published by Awad et al. [46]. About 0.3 gm of CdO powder was dissolved in 1.2 ml of oleic acid. Consecutively, the mixture of oleyl amine (2 ml) and TOPO (2 gm) was investigated with continuous stirring and heating. Once 200 °C was reached, the mixture was injected with 3 ml of pre-dissolved selenium (0.12 gm) and silica powder (0.01 g) in TOP with continuous stirring. Afterward, collecting the obtained samples at different time intervals (2, 5, 7, 10, 15, 20, and 25 min) and labeling them with (S1, S2, S3, S4, S5, S6, and S7).

Each sample was dispersed in 2 ml of toluene, followed by adding 5 ml of methanol. Consequently, the samples were ultracentrifuged to separate the NPs. This technique had to be repeated numerous times to achieve a pure form of CdSe-SiO_2 nanocomposite. Finally, the obtained CdSe-SiO_2 nanocomposites were suspended in hexane (5 ml) followed by drying at 40 °C in a vacuum oven for 12 h and then collecting them in powder forms. The blank SiO_2 was denoted as S0. The occurred chemical reaction is depicted in Fig. 1 as a schematic diagram.

2.3. Characterizations

For the prepared samples of SiO_2 (S0) and CdSe-SiO_2 nanocomposites, the TEM, as well as HR-TEM images, were performed at 200 kV through a transmission electron microscope (Joel JEM-2100). The X-ray diffraction (XRD) was carried out via a standard X′Pert Philips Materials Research diffractometer. XRD spectra were examined in a scan range from 5° to 80°. In the range of wavelengths from 410 to 900 nm, UV-Visible absorption spectra were measured using a double beam spectrophotometer (Perkin Elmer Lambda 40). FTIR spectrometer (Vertex 70, Bruker, Germany), the spectra were recorded in a spectral range of 4000–400 cm^{-1} with a spectral resolution of 4 cm^{-1}.

3. Results and discussion

3.1. TEM analysis

Fig. 2 **(a-c)** reveals the HR-TEM images of the SiO_2 (S0) nanoparticles. It has a sheet-like structure with some agglomerations. The CdSe-SiO_2 nanocomposite (S2) is shown in Fig. 2 **(d-f)**. It reveals that the CdSe QDs were directly grown with a well homogenous distribution and tight attachment to the surface of the SiO_2 sheets, which can keep monodispersity and decrease the surface traps. The average size of the S2 sample is 4.5 nm, as summarized in Table 1.

3.2. XRD analysis

The phase structure of the prepared SiO_2 nanoparticles (S0) and CdSe-SiO_2 nanocomposite (S2) were investigated by XRD, as shown

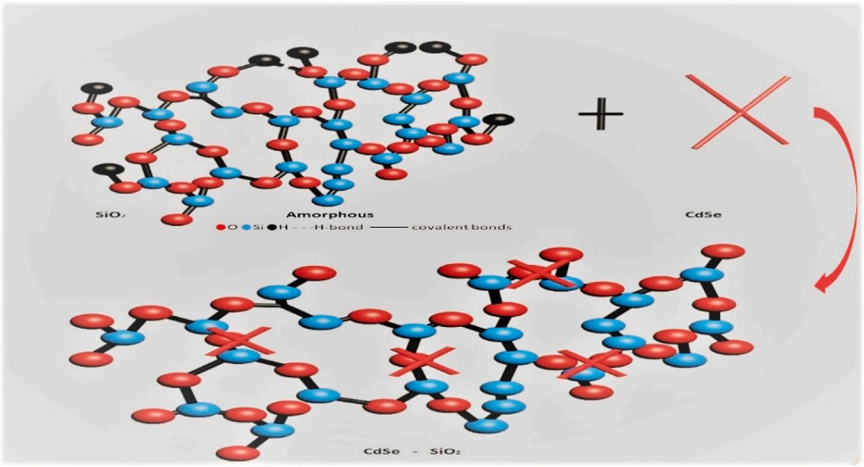

Fig. 1. Schematic representation of the synthesis of CdSe -SiO_2 nanocomposites.

in Fig. 3. XRD spectra in Fig. 3**a** show a broad peak at 2θ = 23°, which is attributed to the amorphous silica. However, the XRD pattern of CdSe-SiO_2, as seen in Fig. 3**b**, shows three distinct peaks at 2θ of 25°,42°, and 50° in (111), (220), and (311) planes, respectively. This is considered strong evidence for the presence of the cubic phase of the CdSe, which has a reference code (JCPDS-XRD Cards no: 04–004–1009). Therefore, it is the reasonable presence of sharp peaks of CdSe and the disappearance of the diffraction peaks of SiO_2 in the XRD pattern of CdSe-SiO_2 nanocomposite [47].

From the XRD humps, the average particle size (M) of the supported CdSe QDs on SiO_2 was estimated using Debye–Scherrer's formula [M= 0.89 λ/B cos(θ)], where λ is the X-ray wavelength, B is the full-width at half-maximum, and θ is the scattering angle [43,48]. The evaluated particle size M for S2 of CdSe QDs on SiO_2 was about 3.4 nm, as seen in Table 1.

The size of nanoparticles was estimated from the peak maxima of the absorption spectra for CdSe QDs on SiO_2 using three theoretical models. One of them is the approach of the Simple Exponential Function (SEF), which was proposed by Bacherikov and his co-workers [49] by using the following formula:

$$S = 0.334\exp\left(\frac{\lambda_{max} - 252.7}{129.3}\right) \quad (1)$$

where S is the particle size's average size. The wavelength of the optical first excitonic absorption peak is λ.

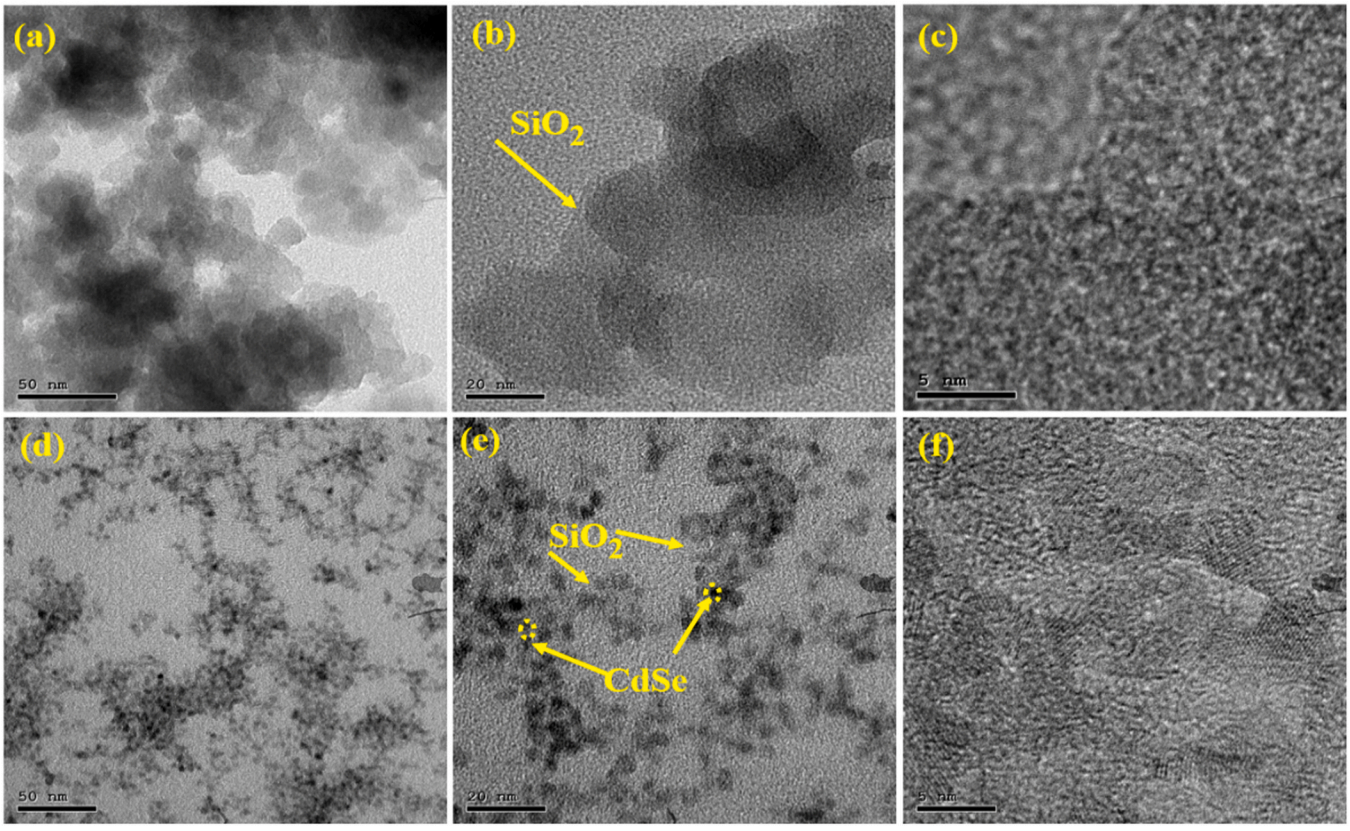

Fig. 2. HR-TEM images of: **(a-c)** the as-prepared SiO_2 nanoparticles (sample S0), and **(d- f)** CdSe-SiO_2 nanocomposite (S2), respectively.

Table 1
The energy gap and the calculated particle size from EMA, SER, PPT, TEM, and X-Ray for the different nanocomposites.

Samples	Energy gap E_g= hc /λ (eV)	Particle size *EMA method* (nm)	Particle size *SEF method* (nm)	Particle size *PFF method* (nm)	Particle size *TEM* (nm)	Particle size *X-RAY* (nm)
S1	2.26	3.55	3.40	3.04	–	–
S2	2.16	3.86	4.19	3.72	4.5	3.40
S3	2.13	3.98	4.42	3.95	–	–
S4	2.10	4.10	4.67	4.20	–	–
S5	2.08	4.19	4.85	4.40	–	–
S6	2.07	4.24	4.97	4.53	–	–
S7	2.06	4.29	5.08	4.66	–	–

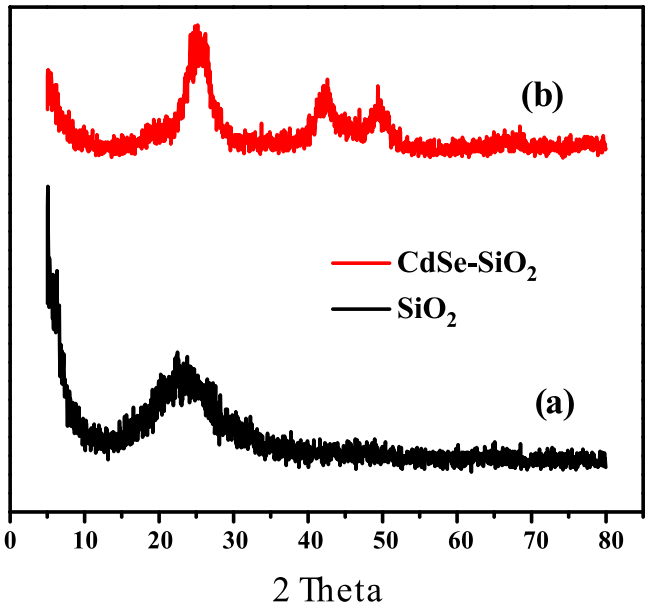

Fig. 3. XRD spectra of **(a)** SiO_2 (S0) and **(b)** CdSe-SiO_2 nanocomposite (S2).

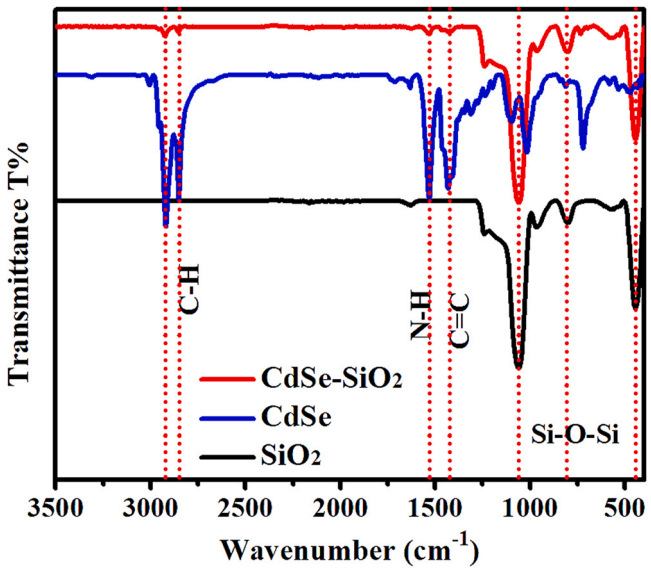

Fig. 4. FTIR spectra of SiO_2, CdSe, and CdSe-SiO_2 nanocomposite.

The second method is known as Polynomial Fitting Functions (*PFF*) [50], which is described by using the particle size D (nm) and the optical excitonic peak λ (nm) through the following relation:

$$D = [1.6122 \times 10^{-9}]\lambda^4 - [2.657 \times 10^{-6}]\lambda^3 + [1.6242 \times 10^{-3}]\lambda^2 - [0.4277]\lambda + [41.57] \quad (2)$$

The Effective Mass Approximation (EMA) [51–53] was the third method used to deduce the size of the prepared nanoparticles by using the following equation:

$$E_{gn} = E_{gb} + \frac{h^2}{8R^2}\left[\frac{1}{m_e} + \frac{1}{m_h}\right] - \frac{1.8e^2}{4\pi\varepsilon\varepsilon_0 R} \quad (3)$$

Where E_{gb} (1.74 eV) is the amount of the bulk crystal bandgap [43,48], E_{gn} is the bandgap value of nanocrystals, R is the radius of the CdSe QDs, m_e is the electron effective mass (0.13 m_o), m_h is the hole effective mass (0.45 m_o; m_o = 9.11 ×10^{-32} kg) and ε is the relative dielectric constant for CdSe QDs [43,48]. The average particle size of CdSe QDs in the CdSe-SiO_2 nanocomposite is estimated using the values of E_{gn} derived from UV spectra in the EMA method. It was found that the average particle size of the nanocomposite using the EMA method (third method) ranged from 3.55 nm for S1 to 4.29 nm for S7, as demonstrated in Table 1. These calculated average particle size values using three theoretical models (SEF, PPT, and EMA) are approximately in the same range as the corresponding values estimated from TEM images and XRD spectra.

3.3. FTIR analysis

FTIR spectra of SiO_2, CdSe, and CdSe- SiO_2 are seen in Fig. 4. FTIR spectra of SiO_2 nanoparticles (S0) showed characteristic peaks at 1060, 802, and 450 cm^{-1}, which corresponded to the symmetrical and asymmetric stretching vibration of Si-O- Si [54,55]. The spectra of FTIR for CdSe QDS showed absorption peaks at 2924 cm^{-1} and 2856 $cm^{-1,}$ which is assigned for the CH_2 stretching vibration modes of the aliphatic hydrocarbons (O.Am and TOPO). However, the absorption peak at 720 cm^{-1} is attributed to the CH_2 deformation of multiple (–(CH_2)n– n ≥ 4) methylene groups of O.Am and TOPO. The bands that appeared at 1530 and 1425 cm^{-1} indicate vibrations of N-H and C═C double bonds of the O.Am. Such results indicate the remaining of O.Am and TOP in their original form after capping with CdSe quantum dots [56]. The FT-IR spectra of the CdSe-SiO_2 nanocomposite (S2) revealed the characteristic peaks of individual nanoparticles that were 1060, 802, and 450 cm^{-1} for SiO_2 and 2924 cm^{-1}, 2856 cm^{-1}, 1530, and 1425 cm^{-1} for CdSe QDs, respectively.

3.4. Optical properties

3.4.1. Absorption, attenuation coefficient, and refractive index

Fig. 5**a** illustrates the variation of absorption spectrum with wavelength for the different nanocomposites of CdSe-SiO_2. For SiO_2 (S0), no absorption peak existed in the range of the studied wavelengths, consistent with a published report [45]. Adding CdSe QDs to SiO_2, with different growth times ranging from 2 to 25 min (increase particle size), caused the appearance of their excitonic peaks in a wavelength range from 550 to 602 nm, as proved in a published

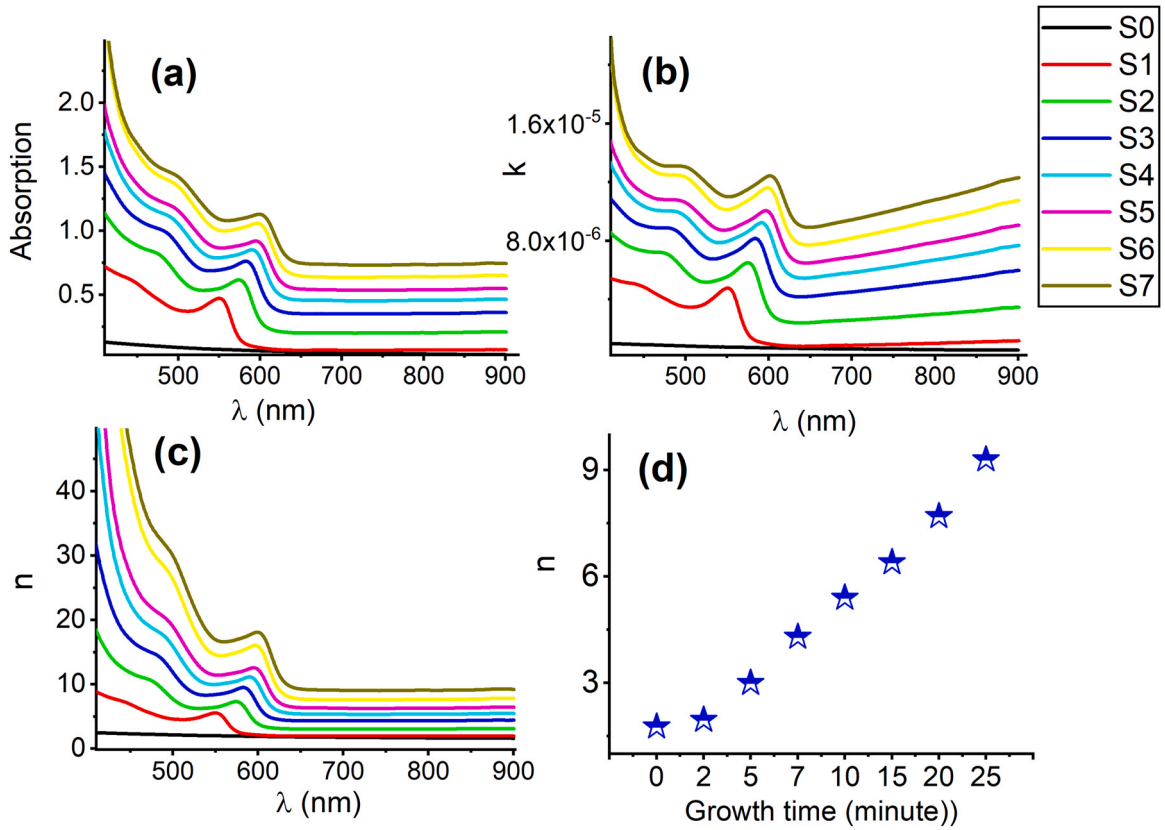

Fig. 5. Dependence of **(a)** spectral absorbance, **(b)** extinction coefficient (k), and **(c)** refractive index (n) on the wavelength (λ) for the studied samples. **(d)** Variation of refractive index (n) with the growth time (min) at 550 nm.

report [57]. The absorption peaks of CdSe-SiO_2 nanocomposites suffered from a redshift (a bathochromic shift) which increases as the growth time of CdSe QDs increases. This behavior can be attributed to the effect of quantum confinement which resulted in grown of particle size of CdSe QDs, as reported previously in some publications [43,47].

One of the most important optical parameters is the extinction coefficient (k) which is determined according to the following relation [58]:

$$k = \frac{\alpha\lambda}{4\pi} \tag{4}$$

Where α is the absorption coefficient (absorbance /thickness), and λ represents the wavelength. Fig. 5**b** shows the extinction coefficient (k) – wavelength dependence for the different nanocomposites of CdSe- SiO_2. Indeed, the extinction coefficient (k) can be used to describe the loss of light energy during its propagation into the studied material due to scattering and absorption per unit distance [59]. Therefore, a high value of k means a high loss of incident light. Increasing the values of k at high wavelengths can be a result of the interaction between the incident electromagnetic radiation and the material of the studied nanocomposites [60]. Fig. 5**b** displays the dependence of the extinction coefficient (k) on the growth time of CdSe QDs /77embedded in SiO_2, as the value of k increases by increasing the growth time. The same behavior ///was observed in Fig. 5**a** due to the reliance of the extinction coefficient (k) on the absorption.

The dispersion of electromagnetic waves of incident light can be described by using the refractive index (n). The extinction coefficient (k) and the reflectance (R) were used to calculate the values of n by using the following relations [61,62]:

$$R = -\sqrt{(Te^{A})} + 1 \tag{5}$$

$$n = \left(\frac{1+R}{1-R}\right) + \sqrt{\frac{4R}{(1-R)^2} - k^2} \tag{6}$$

Where T is the transmission and A is the absorbance. Fig. 5**c** depicts the dependence of the refractive index (n) of the CdSe-SiO_2 nanocomposites on the incident wavelength. The refractive index increased by increasing the wavelength as well as increasing the growth time of CdSe QDs. The refractive index spectrum of SiO_2 (S0) shows a typical normal dispersion as the refractive index increases by decreasing the wavelength [63]. However, the curves of the refractive index of nanocomposites of CdSe -SiO_2 show normal dispersion for the studied range of wavelength except for the strong absorption bands of CdSe QDs in the visible region. The high density of the fabricated nanocomposites and decreasing the interatomic space may explain the improvement of the refractive index of SiO_2 by adding different sizes of CdSe QDs [64]. Also, the excitonic peak positions corresponding to CdSe QDs displayed a bathochromic shift (shift towards a longer wavelength) by increasing their growth time and particle size, in agreement with some literature [65,66]. The enhancement of n values of nanocomposites of CdSe-SiO_2 can candidate them to be usefully applied as antireflection coating for solar cells. Fig. 5**d** illustrates the variation of the refractive index of CdSe-SiO_2 nanocomposites with the growth time (minute) at a wavelength of 550 nm. The determined refractive index values are 1.8, 1.9, 3.0, 4.3, 5.4, 6.4, 7.7, and 9.3, corresponding to the nanocomposites of S0, S1, S2, S3, S4, S5, S6 and S7. It can observe from Fig. 5**d** that the refractive index of the nanocomposites increases linearly as the growth time and CdSe particle size increase. This result gives a strong indication of dispersion of CdSe QDs homogeneously into its nanocomposite with SiO_2 [67].

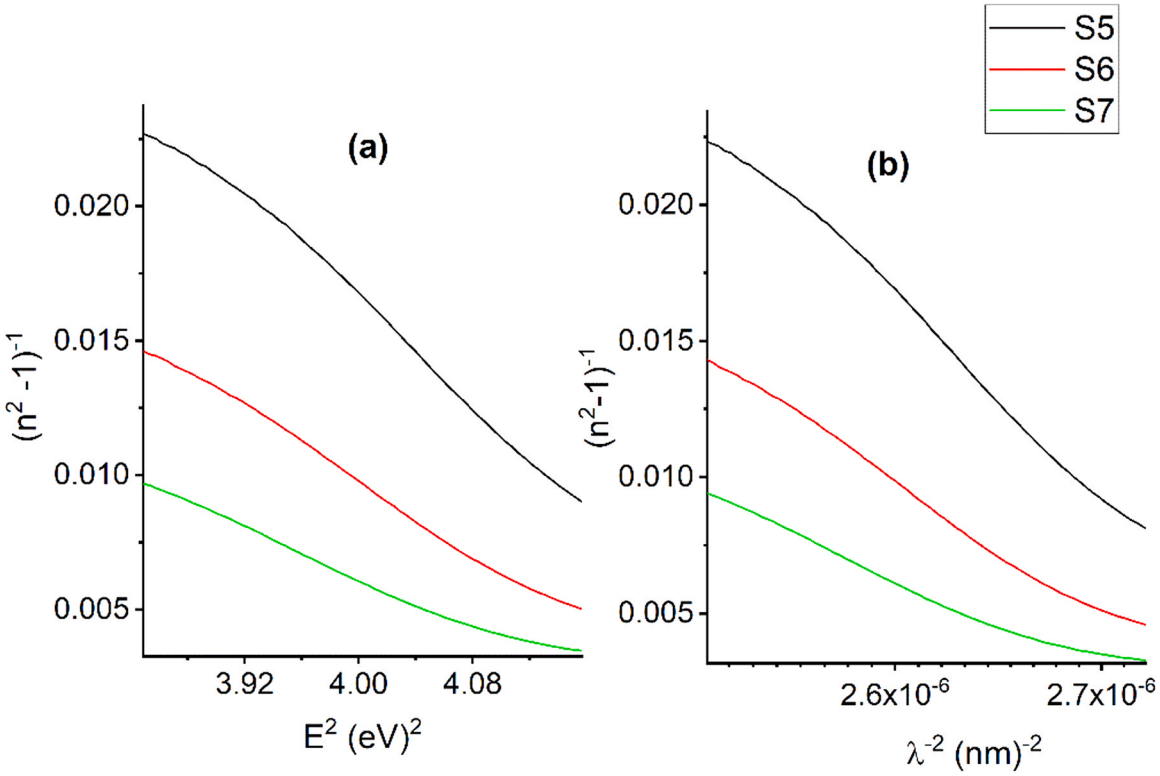

Fig. 6. Plotting **(a)** $(n^2\text{-}1)^{-1}$ versus E^2 and **(b)** $(n^2\text{-}1)^{-1}$ versus λ^{-2} for different nanocomposites.

3.4.2. The Wemple - DiDomenico (W-D) dispersion

The dispersion behavior of the refractive index spectrum was also discussed by the single effective oscillator model of Wemple-DiDomenico (W-D) [68,69] as follows:

$$n^2(E) = 1 + \frac{E_d E_o}{E_o^2 - E^2} \tag{7}$$

where E_o is the single oscillator energy, and E_d is the dispersion energy. The optical dispersion constants of E_d and E_o were determined from $(n^2\text{-}1)^{-1}$ - E^2 plots for the different nanocomposites. Fig. 6**a** displays the variation of $(n^2\text{-}1)^{-1}$ with E^2 for samples of S5, S6, and S7 as examples for the other studied nanocomposites. In Fig. 6**a**, the slope provides the value of $(E_o\,E_d)^{-1}$, whereas the value of (E_o/E_d) was given from the intercept on the vertical axis. Table 2 shows an increase in the values of E_d by increasing the growth time of CdSe QDs, which results in increasing the strength of the interband optical transition of the nanocomposites [70]. Conversely, the single effective oscillator energy (E_o) of the nanocomposites decreased by increasing the growth time of CdSe QDs from 3.06 eV (S0) to 2.07 eV(S7).

The optical oscillator strength (f) can be used to describe the absorption process of photon energy caused by electrons transfer from the initial state to the final state. Therefore, the oscillator strength (f) can effectively give an indication of interaction between the material of the student sample and the incident electromagnetic radiation. The values of f were estimated from the following relation [71]:

$$f = E_o E_d \tag{8}$$

Table 2 includes the deduced values of oscillator strength (f) for the studied nanocomposites. Increasing the growth time of CdSe QDs caused an increase in the values of (f) from 1.81 $(eV)^2$ to 41.7 $(eV)^2$ for S_1 and S_7, respectively, whereas the value of (f) for SiO_2 sample (S0) equals to 12.9 $(eV)^2$.

The optical moments of M_1 and M_3 can also be used to describe the W-D parameters of the optical spectra [72,73]. The optical moments give an indication of the inter-band transition strengths, and they can be calculated according to the following relation [74]:

$$E_o^2 = \frac{M_1}{M_3} \tag{9}$$

$$E_d^2 = \frac{M_1^3}{M_3} \tag{10}$$

The values of M_1 and M_3 for the nanocomposites of CdSe-SiO_2 are listed in Table 2. M_1 and M_3 increased from 0.37 and 0.07, respectively, for S_1 to be 6.62 and 1.54, respectively, for S7. Therefore, increasing the growth time of CdSe QDs was a reason for increasing the optical momentum parameters of the nanocomposites. However, the SiO_2 sample (S0) has values of M_1 and M_3 equal to 1.39 and 0.15, respectively. On the other hand, determining the refractive index at zero photon energy provides a parameter known as static refractive index (n_o), which was calculated by the following relation [75]:

Table 2
The Wemple-Didomenico oscillating parameters including the values of the single oscillator energy (**E_o**), the dispersion energy (**E_d**), the oscillator strength (**f**), the moments of the optical spectrum (**M_1** and **M_3**), the static refractive index (**n_o**), the average interband oscillator wavelength (**λ_o**), the oscillator length strength (**S_o**),a and the long wavelength refractive index (**n_∞**) for the different nanocomposites.

Sample	E_o (eV)	E_d (eV)	f $(eV)^2$	M_1	M_3	n_o	λ_o (nm)	$S_o^* 10^{-6}$ $(nm)^{-2}$	n_∞
S0	3.06	4.24	12.9	1.39	0.15	1.54	416	7.68	2.33
S1	2.22	0.81	1.81	0.37	0.07	1.17	557	1.18	1.37
S2	2.14	1.93	4.13	0.90	0.19	1.38	580	2.73	1.92
S3	2.11	4.12	8.69	1.95	0.44	1.72	586	5.74	2.97
S4	2.10	6.62	13.9	3.15	0.72	2.04	592	9.16	4.21
S5	2.09	9.40	19.6	4.50	1.03	2.35	596	12.5	5.44
S6	2.08	13.8	28.6	6.62	1.54	2.76	599	18.5	7.64
S7	2.07	20.1	41.7	9.71	2.26	3.27	602	26.3	10.5

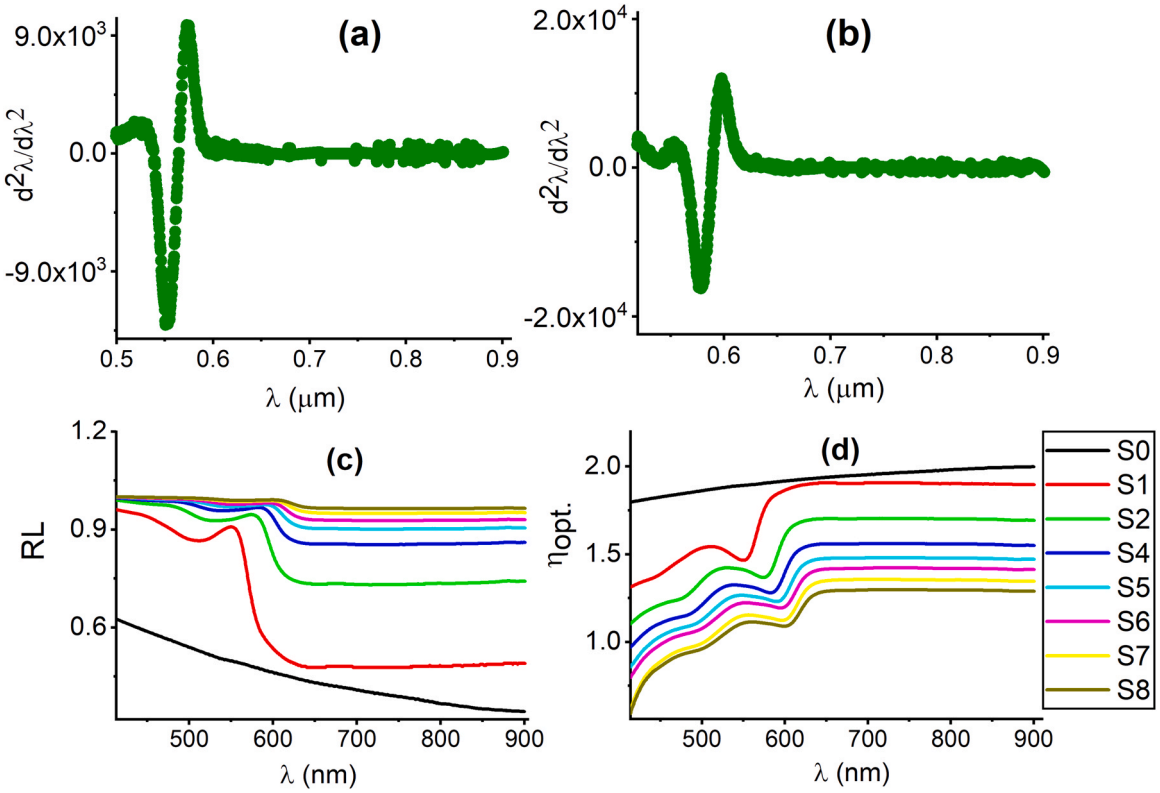

Fig. 7. Variation of the second derivative of refractive index with the wavelength (μm), for samples of **(a)** S1 and **(b)** S2. Dependence of **(c)** the reflection loss (R_L) and **(d)** the optical electronegativity ($\eta_{opt.}$) on wavelength (nm), for all the studied nanocomposites.

$$n_o^2 = 1 + \frac{E_d}{E_o} \tag{11}$$

The values of (n_o) of the nanocomposites, shown in Table 2, prove their dependence on the growth time of CdSe QDs. Moss model was used to determine some important optical parameters according to the following relations [76,77]:

$$\frac{(n_\infty^2 - 1)}{(n^2 - 1)} = 1 - \frac{\lambda_o^2}{\lambda^2} \tag{12}$$

$$n_\infty^2 = 1 + S_o\lambda_o^2 \tag{13}$$

where λ_o describes the average interband oscillator wavelength, S_o is the average oscillator strength and n_∞ is the long-wavelength refractive index. Fig. 6**b** presents the variation of $(n^2 - 1)^{-1}$ with λ^{-2} for nanocomposites of S5, S6, and S7, as examples of the other samples. The slope of the best linear fitting of straight lines in Fig. 6**b** gives a quantity of $1/S_o$ while the quantity of $(S_o^{-1}\,\lambda_o^{-2})$ is obtained from the intercept. Table 2 contains the values of S_o, λ_o, and n_∞ for all the studied nanocomposites. The values of S_o, λ_o and n_∞ are 602 nm, 26.3×10^{-6} $(nm)^{-2}$, and 10.5, respectively, for the S7 sample (growth time of 25 min), which are greater than the corresponding values of the SiO_2 sample (S0) as 416 nm, 7.68×10^{-6} $(nm)^{-2}$ and 2.33, respectively. Therefore, the growth time of CdSe QDs plays an important role in tuning these optical parameters of CdSe-SiO_2 nanocomposites.

3.4.3. Group velocity dispersion (GVD) and dispersion coefficient (D)

The dispersion of the nanocomposites can be understood by estimating the group velocity dispersion (GVD). GVD is known as the frequency dependence of a group velocity in a medium. The values of GVD rely on the second derivation of the refractive index with respect to the incident wavelength according to the following relation [78,79]:

$$GVD = \frac{\lambda^3}{2\pi c^2}\left(\frac{d^2n}{d\lambda^2}\right) \tag{14}$$

The dependence of $(d^2\lambda/d\lambda^2)$ on the incident wavelength (μm) is illustrated in Fig. 7**a** and Fig. 7**b**, corresponding to S1 and S2 nanocomposites, respectively, as examples of the rest samples. Short

Table 3
The group velocity dispersion (GVD), the dispersion coefficient (D), the linear optical susceptibility ($\chi^{(1)}$), the third-order nonlinear optical susceptibility ($\chi^{(3)}$), the nonlinear refractive index (n_2), the ratio of (N_{opt}/m^*), relaxation time (τ), optical mobility ($\mu_{opt.}$) and optical resistivity ($\rho_{opt.}$) for the different nanocomposites.

Sample	GVD ($fs^2/\mu m$)	D ($ps/\mu m^2$)	$\chi^{(1)}$	$\chi^{(3)}$ x 10^{-13} (esu.)	n_2 x10^{-13} (esu.)	($N_{opt.}/m^*$) x 10^{62} (kg^{-1} m^{-3})	τ x 10^{-6} (sec)	$\mu_{opt.}$ x 10^6	$\rho_{opt.}$ x10^{-18}
S_0	–	–	0.11	0.249	6.072	25.8	112.1	44.74	0.0001
S1	3222	-18.7	0.03	0.001	0.044	0.01	0.001	0.0003	33,654
S2	4256	-23.0	0.07	0.041	1.115	0.11	0.003	0.0011	1263.8
S3	5301	-26.8	0.16	1.114	24.44	0.37	0.006	0.0025	170.59
S4	5884	-29.8	0.25	6.641	122.7	1.24	0.017	0.0067	18.673
S5	6291	-31.9	0.36	28.55	458.5	2.94	0.034	0.0137	3.8830
S6	8117	-39.8	0.53	134.1	1830	166	1.166	0.4656	0.0020
S7	8379	-41.1	0.77	597.6	6881	167	1.180	0.4711	0.0019

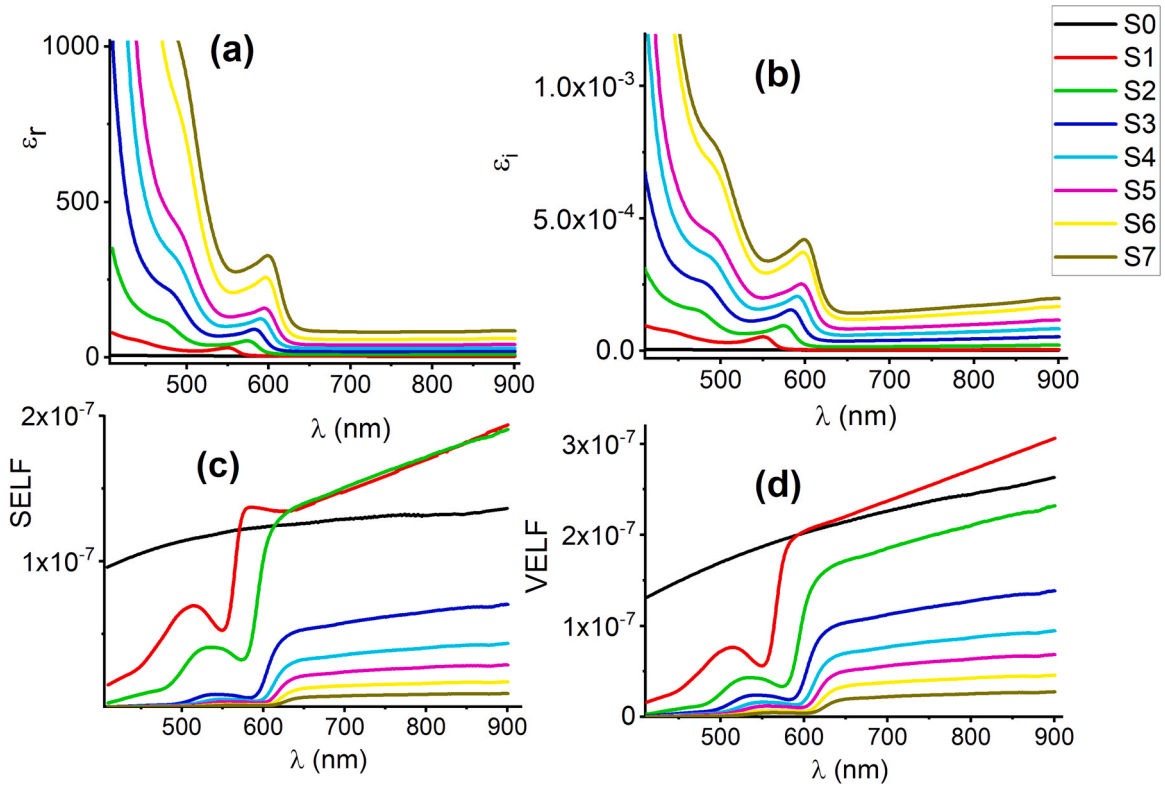

Fig. 8. Dependence of **(a)** real part of dielectric constant (ε_r) and **(b)** imaginary part of dielectric constant (ε_i), **(c)** the surface energy loss function (SELF), and **(d)** the volume energy loss function (VELF) on the wavelength (λ), for the different nanocomposites.

pulses of light are observed in Fig. 7 **(a&b),** which spread in time due to the traveling of variant frequency components of the pulse at some diverse velocities. Increasing the growth time of CdSe QDs caused an obvious enhancement of GVD values, as displayed in Table 3. In addition, the broadening of optical pulses caused by dispersion in the material of the tested medium can be expressed by the dispersion parameter (D), which is related to GVD by the following relation [79]:

$$D = -\frac{\lambda}{c}\left(\frac{d^2n}{d\lambda^2}\right) = \frac{-2\pi c}{\lambda^2}GVD \tag{15}$$

The negative values of D, listed in Table 3, give an indication that all CdSe -SiO_2 nanocomposites have positive dispersion mediums.

3.4.4. The reflection loss factor (RL) and the optical electronegativity (η_{opt})

The following equation was used to calculate the values of the reflection loss factor (RL) for all the prepared samples [59]:

$$R_L = \frac{(n^2-1)}{(n^2+2)} \tag{16}$$

Fig. 7**c** shows the variation of RL with wavelength for all the nanocomposites. At constant wavelength of 700 nm, RL has values of 0.41, 0.47, 0.73, 0.85, 0.89, 0.92, 0.95 and 0.97, corresponding to samples of S0, S1, S2, S3, S4, S5, S6 and S7, respectively. On the other hand, the optical electronegativity (η_{opt}), which is an indicator of an ionic bond creation by atom or radial attraction, can be expressed as the following [80]:

$$\eta_{opt} = (An^{-1})^{\frac{1}{4}} \tag{17}$$

where A is a constant and has a value of 25.54 for most of the substances [81]. Plotting η_{opt} with wavelength for the different nanocomposites is displayed in Fig. 7**d**. For nanocomposites of S0, S1, S2, S3, S4, S5, S6, and S7, the values of η_{opt} are 1.95, 1.90, 1.7, 1.56, 1.48, 1.42, 1.36 and 1.29, respectively. Consequently, increasing the growth time of CdSe QDs resulted in increasing the reflection loss factor (RL) and decreasing the optical electronegativity (η_{opt}).

3.4.5. Optical dielectric constants

The real part (ε_r) and the imaginary part (ε_i) of complex dielectric function are related to each other by the following equation:

$$\varepsilon^* = \varepsilon_r + i\varepsilon_i \tag{18}$$

where ε_r relies on the motion of electrons during light transformation in the medium, and ε_i contributes to the dissipative rate of light during its transmission within a material. The real and imaginary parts of complex dielectric function can be expressed in terms of refractive index (n) and extinction coefficient (k) as the following [82]:

$$\varepsilon_r = n^2 - k^2; \varepsilon_i = 2nk \tag{19}$$

Fig. 8 **(a&b)** illustrates the plotting of ε_r and ε_i, respectively, versus the wavelength (λ), for all the nanocomposites of CdSe-SiO_2. The dispersion and dissipative rates of light within a material were described by the estimated values of ε_r and ε_i, respectively. They can also describe the electron-photon interaction within the materials of the studied nanocomposites. The same behavior of k and n curves, in Fig. 5 **(b &c)**, were observed for ε_r and ε_i plots, in Fig. 8 **(a & b)**, since the optical dielectric parameters depend on n and k values. Also, increasing the growth time of CdSe QDs was a reason for the enhancement in the values of (ε_r) and (ε_i) and also the observed redshift in the peak positions.

3.4.6. Functions of energy loss

This study included two types of energy loss functions which are surface energy loss function (SELF) and volume energy loss function (VELF). SELF describes the energy loss probability of fast electrons

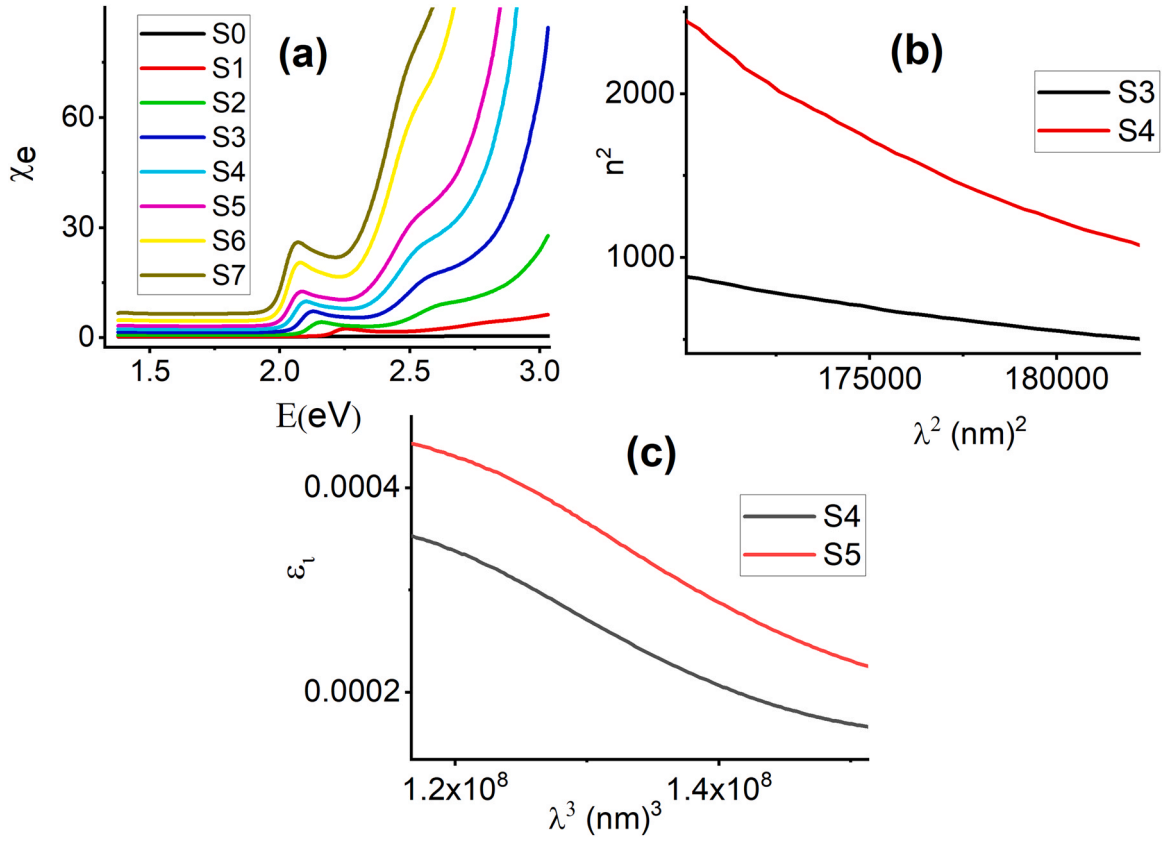

Fig. 9. Plotting of **(a)** the linear electrical susceptibility (χ_e) versus the photon energy (E), for the different nanocomposites, **(b)** n^2 versus $\lambda^{2,}$ and **(c)** ε_i versus λ^3, for some different nanocomposites.

during their traveling on a material surface. Nevertheless, missing the fast electron their energies when they propagate through a material can be termed by VELF. The real and imaginary parts of complex dielectric were used to deduce the values of SELF and VELF as the following relations [83]:

$$SELF = \frac{\varepsilon_i}{(\varepsilon_r + 1)^2 + \varepsilon_i^2}; VELF = \frac{\varepsilon_i}{\varepsilon_r^2 + \varepsilon_i^2} \quad (20)$$

Fig. 8 **(c&d)** represents the variation of SELF and VELF, respectively, with the incident wavelength, for all the nanocomposites. The values of VELF are greater than the values of SELF for the same studied nanocomposites. Consequently, the fast electrons miss their energies through their propagation within the studied materials more than through traveling on their surfaces. Fig. 8 **(c&d)** show that SELF and VELF increase by increasing the incident wavelength except for the positions of excitonic peaks (observed in Fig. 5**a**), in which they decreased and shifted to a longer wavelength. In addition, the values of SELF and VELF were CdSe growth time-dependent.

3.4.7. Electrical, linear, and nonlinear optical susceptibilities and the non-linear refractive index

Deducing linear optical susceptibility ($\chi^{(1)}$) can help in understanding the response of a material to incident electromagnetic energy. The linear optical susceptibility was calculated from the following formula [84]:

$$\chi^{(1)} = \frac{E_d}{4\pi E_o} \quad (21)$$

The theoretical Tichy and Ticha model [85] was used to study some nonlinear parameters in which the W-D parameter is combined with the rule of Miller [76]. One of the most important nonlinear optical parameters used for some optical applications is the third nonlinear susceptibility ($\chi^{(3)}$). It gives an indicator of the degree of nonlinearities, and it was calculated from the following formula [86]:

$$\chi^{(3)} = A[\chi^{(1)}]^4 \quad (22)$$

where A is the frequency-independent constant which equals 1.7×10^{-10} (e.s.u) for all the materials [87].

According to Miller's rule, the static refractive index (n_o), as well as the third nonlinear susceptibility ($\chi(3)$), can be used to calculate the non-linear refractive index (n_2) as the following [85,88]:

$$n_2 = \frac{12\pi\chi^{(3)}}{n_o} \quad (23)$$

Table 3 shows the calculated values of linear optical susceptibility ($\chi^{(1)}$), the third nonlinear susceptibility ($\chi^{(3)}$), and the non-linear refractive index (n_2) for all the nanocomposites of CdSe -SiO_2. The growth time of CdSe QDs played a significant role in improving the values of $\chi^{(1)}$, $\chi^{(3),}$ and n_2 of the nanocomposites. The high values of n_2 of the nanocomposites may nominate them to be usefully used in optical applications such as ultrafast switching and telecommunications.

On the other hand, the electrical susceptibility (χ_e) was calculated to describe the electric behavior of the studied materials under electric field application. The following equation was used to determine the values of the electrical susceptibility (χ_e) [89,90]:

$$\chi_e = \frac{(n^2 - k^2 - \varepsilon_o)}{4\pi} \quad (24)$$

The variation of χ_e with the photon energy (E) for the variant nanocomposites is presented in Fig. 9**a**. It can observe that the values of the electrical susceptibility (χ_e) of the nanocomposites increase by increasing the incident photon energy. This behavior can be

attributed to increasing electron mobility [91]. Also, the CdSe growth time can develop the electrical susceptibility (χ_e) of the nanocomposites.

3.4.8. The ratio of (N_{opt}/m^*), relaxation time, optical mobility, and optical resistivity

The free electron and also the bound electrons can partially affect the dielectric constant of a material according to the following formula [71]:

$$n^2 = \varepsilon_\infty - \frac{1}{4\pi^2\varepsilon_o}\left(\frac{e^2}{c^2}\right)\left(\frac{N_{opt}}{m^*}\right)\lambda^2 \quad (25)$$

Where ε_∞ is the high-frequency dielectric constant, e is the electronic charge, N_{opt} is the number of the carrier concentrations, ε_o is the free space permittivity, c is the speed of light waves, and m^* is the effective mass of the charge carriers. The ratio of (N_{opt}/m^*) was obtained for the nanocomposites from the slope of the plot of n^2 versus the square of wavelength (λ^2), as shown in Fig. 9**b** for the samples of S3 and S4, as examples for the others. The listed values of (N_{opt}/m^*) for the different samples in Table 3 prove their dependence on the CdSe growth time.

The Drude model of the free electron was studied by using the results of the imaginary part of the dielectric constant (ε_i) as the following relation [92].

$$\varepsilon_i = \frac{1}{4\pi^3\varepsilon_o}\left(\frac{e^2}{c^3}\right)\left(\frac{N_{opt}}{m^*}\right)\left(\frac{1}{\tau}\right)\lambda^3 \quad (26)$$

where τ is the relaxation time. The variation of ε_i with $\lambda^3$is depicted in Fig. 9**c** for samples of S4 and S5, as examples for the rest nanocomposites. The slopes of the straight lines in Fig. 9**c** provide the quantity of $\left\{\frac{1}{4\pi^3\varepsilon_o}\left(\frac{e^2}{c^3}\right)\left(\frac{N_{opt}}{m^*}\right)\left(\frac{1}{\tau}\right)\right\}$. The relaxation time was deduced using the previously tabulated values of $\left(\frac{N_{opt}}{m^*}\right)$ and they were reported, for all the nanocomposites, in Table 3.

The optical mobility (μ_{opt}) and optical resistivity (ρ_{opt}) were determined by using the values of the charge carrier concentrations (N_{opt}) and the relaxation time (τ) as the following [59]:

$$\mu_{opt} = \frac{e\tau}{m^*}; \rho_{opt} = \frac{1}{e\mu_{opt}N_{opt}} \quad (27)$$

where the effective mass of the charge carriers (m^*) equals 0.44 m_o [93]. All the values of the optical mobility (μ_{opt}) and the optical resistivity (ρ_{opt}) for all the nanocomposites are described in Table 3. The values of τ and μ_{opt} of the nanocomposites increased by increasing the growth time of CdSe QDs whereas the corresponding values for SiO_2 were higher than all those of the nanocomposites. On the other hand, the values of the optical resistivity (ρ_{opt}) of the nanocomposites decreased by increasing the growth time of CdSe QDs while the corresponding value of SiO_2 was less than all of them.

4. Conclusion

The effect of different growth times of CdSe was studied on the optical properties of its nanocomposites with SiO_2 NPs. The TEM images prove that the CdSe QDs are homogeneously distributed and well attached to the surface of the SiO_2 sheets. The XRD confirms the phase structure of the as-prepared CdSe QDs, which were grown on the surface of the SiO_2. Also, the FT-IR spectra confirm the formation of the CdSe-SiO_2 nanocomposite. The negative values of the dispersion parameter (D) give an indication that all CdSe -SiO_2 nanocomposites have positive dispersion mediums. The values of S_o, λ_o and n_∞ are 602 nm, 26.3×10^{-6} $(nm)^{-2}$, and 10.5, respectively, for the S7 sample (growth time of 25 min). These values are greater than the corresponding values of the SiO_2 sample (S0), which are 416 nm, 7.68×10^{-6} $(nm)^{-2}$, and 2.33, respectively. The values of τ and μ_{opt} of the nanocomposites increased by increasing the growth time of CdSe QDs, whereas the corresponding values for SiO_2 were higher than all the nanocomposites. Also, the CdSe growth time can develop the electrical susceptibility (χ_e) of the nanocomposites. Increasing the growth time (particle size) of CdSe QDs was a reason for the enhancement in the values of ε_r and ε_i and also the observed redshift in the peak positions. Therefore, the growth time of CdSe QDs plays an important role in tuning the optical parameters of CdSe-SiO_2 nanocomposites.

CRediT authorship contribution statement

Ahmed I. Abdel-Salam: Conceptualization, Methodology, Formal analysis, Data curation, Writing – original draft. **A. Khalid**: Conceptualization, Formal analysis, Investigation, Writing – review & editing. **M.M. Awad**: Conceptualization, Methodology, Formal analysis, Data curation, Writing – original draft. **Yasmein Hussein**: Conceptualization, Methodology, Data curation, Resources, Writing – review & editing. **R.M. Ahmed**: Conceptualization, Formal analysis, Investigation, Writing – review & editing.

Data availability

The data that has been used is confidential.

Declaration of Competing Interest

The authors declare that they have no known competing financial interests or personal relationships that could have appeared to influence the work reported in this paper.

References

[1] L. Zhang, et al., Nano-designed semiconductors for electro-and photoelectro-catalytic conversion of carbon dioxide, Chem. Soc. Rev. 47 (14) (2018) 5423–5443.
[2] K.M. Koo, et al., Merging new-age biomarkers and nanodiagnostics for precision prostate cancer management, Nat. Rev. Urol. 16 (5) (2019) 302–317.
[3] S.H. Lee, B.-H. Jun, Silver nanoparticles: synthesis and application for nanomedicine, Int. J. Mol. Sci. 20 (4) (2019) 865.
[4] W.-Y. Rho, et al., Recent advances in plasmonic dye-sensitized solar cells, J. Solid State Chem. 258 (2018) 271–282.
[5] E. Hahm, et al., Multilayer Ag-embedded silica nanostructure as a surface-enhanced raman scattering-based chemical sensor with dual-function internal standards, ACS Appl. Mater. Interfaces 10 (47) (2018) 40748–40755.
[6] H.-M. Kim, et al., Assembly of plasmonic and magnetic nanoparticles with fluorescent silica shell layer for tri-functional SERS-magnetic-fluorescence probes and its bioapplications, Sci. Rep. 8 (1) (2018) 1–10.
[7] X.-H. Pham, et al., Enzyme-catalyzed Ag growth on Au nanoparticle-assembled structure for highly sensitive colorimetric immunoassay, Sci. Rep. 8 (1) (2018) 1–7.
[8] K.-Y. Lee, et al., Introduction of nanobiotechnology, Nanotechnology for Bioapplications, Springer, 2021, pp. 1–22.
[9] S.-m Park, et al., Towards clinically translatable in vivo nanodiagnostics, Nat. Rev. Mater. 2 (5) (2017) 1–20.
[10] I.L. Medintz, et al., Quantum dot bioconjugates for imaging, labelling and sensing, Nat. Mater. 4 (6) (2005) 435–446.
[11] X.-H. Pham, et al., Synthesis and application of silica-coated quantum dots in biomedicine, Int. J. Mol. Sci. 22 (18) (2021) 10116.
[12] A.I. Abdel-Salam, et al., Anisotropic CuInSe2 nanocrystals: synthesis, optical properties and their effect on photoelectric response of dye-sensitized solar cell, Rev. Mex. Física 66 (1) (2020) 14–22.
[13] M. Bruchez Jret al., Semiconductor nanocrystals as fluorescent biological labels, Science 281 (5385) (1998) 2013–2016.
[14] H. Lee, et al., CdSe tetrapod interfacial layer for improving electron extraction in planar heterojunction perovskite solar cells, Nanotechnology 30 (6) (2018) 065401.
[15] V. Klimov, et al., Optical gain and stimulated emission in nanocrystal quantum dots, Science 290 (5490) (2000) 314–317.
[16] R. Nashed et al., Detailed Study of Different CuInSe2 Nanocrystal Shapes and Their Effect on the Photocurrent Response of Dye-Sensitized Solar Cells, in: Asia Communications and Photonics Conference, 2012. Optical Society of America.
[17] R. Nashed et al., Remarkable Enhancement of the Photocurrent Response of Dye-Sensitized Solar Cells using CuInSe2 Nanocrystals, in: Asia Communications and Photonics Conference, 2012. Optical Society of America.

[18] S. Tripathi, R. Kaur, Investigation of non-linear optical properties of CdS/PS polymer nanocomposite synthesized by chemical route, Opt. Commun. 352 (2015) 55–62.
[19] J.G. Croissant, et al., Synthetic amorphous silica nanoparticles: toxicity, biomedical and environmental implications, Nat. Rev. Mater. 5 (12) (2020) 886–909.
[20] W.M. Haynes, D.R. Lide, T. Bruno, Abundance of elements in the earth's crust and in the sea, CRC Handb. Chem. Phys. 97 (2402) (2016) 14–17.
[21] P.J. Heaney, Structure and chemistry of the low-pressure silica polymorphs, Silica, De Gruyter, 2018, pp. 1–40.
[22] K.R. Iler, The chemistry of silica. Solubility, polymerization, colloid and surface properties and biochemistry of silica, 1979.
[23] S.C. Jana, S. Jain, Dispersion of nanofillers in high performance polymers using reactive solvents as processing aids, Polymer 42 (16) (2001) 6897–6905.
[24] S. Mallakpour, Z. Khani, Fabrication of poly (vinyl alcohol) nanocomposites having different contents of modified SiO2 by vitamin B1 as biosafe and novel coupling agent to improve mechanical and thermal properties, Polym. Compos. 39 (S3) (2018) E1589–E1597.
[25] K. Chrissafis, et al., Thermal and dynamic mechanical behavior of bionanocomposites: fumed silica nanoparticles dispersed in poly (vinyl pyrrolidone), chitosan, and poly (vinyl alcohol), J. Appl. Polym. Sci. 110 (3) (2008) 1739–1749.
[26] X. Zhang, et al., Double-layered TiO2− SiO2 nanostructured films with self-cleaning and antireflective properties, J. Phys. Chem. B 110 (50) (2006) 25142–25148.
[27] C.S. Thompson, R.A. Fleming, M. Zou, Transparent self-cleaning and antifogging silica nanoparticle films, Sol. Energy Mater. Sol. Cells 115 (2013) 108–113.
[28] T. Aubert, et al., Bright and stable CdSe/CdS@SiO2 nanoparticles suitable for long-term cell labeling, ACS Appl. Mater. Interfaces 6 (14) (2014) 11714–11723.
[29] K. Zhao, Z. Pan, X. Zhong, Charge recombination control for high efficiency quantum dot sensitized solar cells, J. Phys. Chem. Lett. 7 (3) (2016) 406–417.
[30] J. Yang, et al., Suppressed interfacial charge recombination of PbS quantum dot photovoltaics by graphene incorporated into ZnO nanoparticles, ACS Appl. Mater. Interfaces 10 (30) (2018) 25311–25320.
[31] W. Wang, et al., Cosensitized quantum dot solar cells with conversion efficiency over 12%, Adv. Mater. 30 (11) (2018) 1705746.
[32] H.-J. Son, et al., Glass-encapsulated light harvesters: more efficient dye-sensitized solar cells by deposition of self-aligned, conformal, and self-limited silica layers, J. Am. Chem. Soc. 134 (23) (2012) 9537–9540.
[33] E. Palomares, et al., Control of charge recombination dynamics in dye sensitized solar cells by the use of conformally deposited metal oxide blocking layers, J. Am. Chem. Soc. 125 (2) (2003) 475–482.
[34] A.K. Chandiran, M.K. Nazeeruddin, M. Grätzel, The role of insulating oxides in blocking the charge carrier recombination in dye-sensitized solar cells, Adv. Funct. Mater. 24 (11) (2014) 1615–1623.
[35] J. Liu, et al., A novel ZnS/SiO2 double passivation layers for the CdS/CdSe quantum dots co-sensitized solar cells based on zinc titanium mixed metal oxides, Sol. Energy Mater. Sol. Cells 208 (2020) 110380.
[36] N. Liu, P. Yang, Photoluminescence properties of hybrid SiO2–coated CdTe/CdSe quantum dots, Luminescence 29 (6) (2014) 566–572.
[37] H. Liu, X. Wang, D. Wu, Tailoring of bifunctional microencapsulated phase change materials with CdS/SiO2 double-layered shell for solar photocatalysis and solar thermal energy storage, Appl. Therm. Eng. 134 (2018) 603–614.
[38] M. Ahmed, M. Abdel-Messih, E.H. Ismail, Facile synthesis of novel microporous CdSe/SiO2 nanocomposites selective for removal of methylene blue dye by tandem adsorption and photocatalytic process, J. Mater. Sci. Mater. Electron. 30 (19) (2019) 17527–17539.
[39] L.L. Beecroft, C.K. Ober, Nanocomposite materials for optical applications, Chem. Mater. 9 (6) (1997) 1302–1317.
[40] T. Soliman, S. Vshivkov, S.I. Elkalashy, Structural, linear and nonlinear optical properties of Ni nanoparticles–Polyvinyl alcohol nanocomposite films for optoelectronic applications, Opt. Mater. 107 (2020) 110037.
[41] K. Iliopoulos, et al., Multifunctional Bi2ZnOB2O6 single crystals for second and third order nonlinear optical applications, Appl. Phys. Lett. 103 (23) (2013) 231103.
[42] A. Zawadzka, et al., Structural and nonlinear optical properties of as-grown and annealed metallophthalocyanine thin films, Thin Solid Films 545 (2013) 429–437.
[43] A.I. Abdel-Salam, et al., The effect of graphene on structure and optical properties of CdSe nanoparticles for optoelectronic application, J. Alloy. Compd. 898 (2022) 162946.
[44] T.S. Soliman, S.A. Vshivkov, S.I. Elkalashy, Structural, thermal, and linear optical properties of SiO2 nanoparticles dispersed in polyvinyl alcohol nanocomposite films, Polym. Compos. 41 (8) (2020) 3340–3350.
[45] H.A. Badran, et al., Thermal blooming and photoluminescence characterizations of sol–gel CdO–SiO2 with different nanocomposite, J. Mater. Sci. Mater. Electron. 27 (3) (2016) 2212–2220.
[46] M.M. Awad, et al., Tuning the optical properties of CdSe quantum dot using graphene nanocomposite, J. Opt. 48 (4) (2019) 616–625.
[47] H.E. ElZorkany, et al., Monitoring the cellular uptake of silica-coated CdSe/ZnS quantum dots by time lapse confocal laser scanning microscopy, J. Appl. Pharm. Sci. 8 (03) (2018) 001–008.
[48] A.I. Abdel-Salam, et al., Facile one-step hydrothermal method for NiCo2S4/rGO nanocomposite synthesis for efficient hybrid supercapacitor electrodes, Mater. Chem. Phys. 277 (2022) 125554.
[49] J.W. Kyobe, et al., CdSe quantum dots capped with naturally occurring biobased oils, New J. Chem. 39 (9) (2015) 7251–7259.
[50] W.W. Yu, et al., Experimental determination of the extinction coefficient of CdTe, CdSe, and CdS nanocrystals, Chem. Mater. 15 (14) (2003) 2854–2860.
[51] O. Madelung, Semiconductors—Basic Data, Springer Science & Business Media, 2012.
[52] R. Sathyamoorthy, et al., Low temperature synthesis of thiol-functionalized CdTe nanoclusters with different tellurium contents, Cryst. Res. Technol. J. Exp. Ind. Crystallogr. 45 (1) (2010) 99–103.
[53] C.P. Shah, et al., Precursor concentration and temperature controlled formation of polyvinyl alcohol-capped CdSe-quantum dots, Beilstein J. Nanotechnol. 1 (1) (2010) 119–127.
[54] R. Dong, et al., A novel SiO2–GO/acrylic resin nanocomposite: fabrication, characterization and properties, Appl. Phys. A 125 (8) (2019) 1–11.
[55] T.N. Tran, et al., Synthesis of amorphous silica and sulfonic acid functionalized silica used as reinforced phase for polymer electrolyte membrane, Adv. Nat. Sci. Nanosci. Nanotechnol. 4 (4) (2013) 045007.
[56] N. Órdenes-Aenishanslins, et al., Biological synthesis of CdS/CdSe core/shell nanoparticles and its application in quantum dot sensitized solar cells, Front. Microbiol. (2019) 1587.
[57] T. Trindade, M. Neves, A. Barros, Preparation and optical properties of CdSe/polymer nanocomposites, Scr. Mater. 43 (6) (2000) 567–571.
[58] R. Ahmed, Optical study on poly (methyl methacrylate)/poly (vinyl acetate) blends, Int. J. Photoenergy (2009) **2009**.
[59] R. Ahmed, T. Taha, F. Ezz-Eldin, Investigation of Sm2O3 effect on opto-electrical parameters and dielectric properties of some fluorophosphate glasses, J. Mater. Sci. Mater. Electron. 32 (24) (2021) 28919–28934.
[60] S.B. Aziz, et al., Optical properties of pure and doped PVA: PEO based solid polymer blend electrolytes: two methods for band gap study, J. Mater. Sci. Mater. Electron. 28 (10) (2017) 7473–7479.
[61] A. El Sayed, et al., Synthesis, characterization, optical, and dielectric properties of polyvinyl chloride/cadmium oxide nanocomposite films, Polym. Compos. 35 (9) (2014) 1842–1851.
[62] A. El Sayed, W. Morsi, Dielectric relaxation and optical properties of polyvinyl chloride/lead monoxide nanocomposites, Polym. Compos. 34 (12) (2013) 2031–2039.
[63] H. Bach, N. Neuroth, The Properties of Optical Glass, Springer Science & Business Media, 1998.
[64] M. Abdelaziz, Cerium (III) doping effects on optical and thermal properties of PVA films, Phys. B Condens. Matter 406 (6–7) (2011) 1300–1307.
[65] V. Zucolotto, et al., Nanoscale manipulation of CdSe quantum dots in layer-by-layer films: influence of the host polyelectrolyte on the luminescent properties, Appl. Surf. Sci. 246 (4) (2005) 397–402.
[66] N.A. Hamizi, M.R. Johan, Optical properties of CdSe quantum dots via non-TOP based route, Int. J. Electrochem. Sci. 7 (9) (2012) 8458–8467.
[67] Y. Rao, S. Chen, Molecular composites comprising TiO2 and their optical properties, Macromolecules 41 (13) (2008) 4838–4844.
[68] S. Wemple, M. DiDomenico Jr, Behavior of the electronic dielectric constant in covalent and ionic materials, Phys. Rev. B 3 (4) (1971) 1338.
[69] R. Ahmed, A.A. Ibrahiem, E.A. El-sayd, Effect of cobalt chloride on the optical properties of PVA/PEG blend, Arab. J. Nucl. Sci. Appl. 52 (1) (2019) 22–32.
[70] M. Ghanipour, D. Dorranian, Effect of Ag-nanoparticles doped in polyvinyl alcohol on the structural and optical properties of PVA films, J. Nanomater. (2013) **2013**.
[71] A. Ali, et al., Optical and dielectric results of Y0. 225Sr0. 775CoO3 ± δ thin films studied by spectroscopic ellipsometry technique, Results Phys. (3) (2013) 167–172.
[72] F. Yakuphanoglu, H. Erten, Refractive index dispersion and analysis of the optical constants of an ionomer thin film, Opt. Appl. 35 (2005) 4.
[73] S. Wemple, M. DiDomenico Jr, Optical dispersion and the structure of solids, Phys. Rev. Lett. 23 (20) (1969) 1156.
[74] M. Frumar, et al., Optically and thermally induced changes of structure, linear and non-linear optical properties of chalcogenides thin films, J. Non-Cryst. Solids 326 (2003) 399–404.
[75] K. Tanaka, Optical properties and photoinduced changes in amorphous As S films, Thin Solid films 66 (3) (1980) 271–279.
[76] S. Wemple, Refractive-index behavior of amorphous semiconductors and glasses, Phys. Rev. B 7 (8) (1973) 3767.
[77] R. Ahmed, A. Ibrahiem, E. El-Said, Effect of cobalt chloride as filler and PVP on the optical properties of PVA/PEG/PVP blends, Opt. Spectrosc. 128 (5) (2020) 642–655.
[78] R. Ahmed, M. Atta, E. Taha, Optical spectroscopy, thermal analysis, and dynamic mechanical properties of graphene nano-platelets reinforced polyvinylchloride, J. Mater. Sci. Mater. Electron. 32 (17) (2021) 22699–22717.
[79] R.J. Lanzafame, Ultrashort laser pulse phenomena: fundamentals, techniques, and applications on a femtosecond time scale, by Jean-Claude Diels and Wolfgang Rudolph, Photomed. Laser Ther. 25 (1) (2007) 58-58.
[80] J. Duffy, Trends in energy gaps of binary compounds: an approach based upon electron transfer parameters from optical spectroscopy, J. Phys. C Solid State Phys. 13 (16) (1980) 2979.
[81] R. Reddy, et al., Correlation between optical electronegativity and refractive index of ternary chalcopyrites, semiconductors, insulators, oxides and alkali halides, Opt. Mater. 31 (2) (2008) 209–212.
[82] R. Ahmed, A. Ibrahim, E. El-Said, Enhancing the optical properties of polyvinyl alcohol by blending it with polyethylene glycol, Acta Phys. Pol. A 137 (2020) 3.
[83] S. Sarkar, N. Das, K. Chattopadhyay, Optical constants, dispersion energy parameters and dielectric properties of ultra-smooth nanocrystalline BiVO4 thin films prepared by rf-magnetron sputtering, Solid State Sci. 33 (2014) 58–66.

[84] S.E. Fritz, T.W. Kelley, C.D. Frisbie, Effect of dielectric roughness on performance of pentacene TFTs and restoration of performance with a polymeric smoothing layer, J. Phys. Chem. B 109 (21) (2005) 10574–10577.
[85] H. Ticha, L. Tichy, Semiempirical relation between non-linear susceptibility (refractive index), linear refractive index and optical gap and its application to amorphous chalcogenides, J. Optoelectron. Adv. Mater. 4 (2) (2002) 381–386.
[86] A.A. Ziabari, F. Ghodsi, Optoelectronic studies of sol–gel derived nanostructured CdO–ZnO composite films, J. Alloy. Compd. 509 (35) (2011) 8748–8755.
[87] P. Zhou, et al., Annealing effect of linear and nonlinear optical properties of Ag: Bi 2 O 3 nanocomposite films, Opt. Express 13 (5) (2005) 1508–1514.
[88] E. Shaaban, et al., Structural, linear and non-linear optical properties of annealed As47. 5Se47. 5Ag5 thin films for optoelectronic applications, Opt. Mater. (86) (2018) 318–325.
[89] V. Gupta, A. Mansingh, Influence of postdeposition annealing on the structural and optical properties of sputtered zinc oxide film, J. Appl. Phys. 80 (2) (1996) 1063–1073.
[90] S.A. Gad, et al., Influence of Fe2O3 dopant on dielectric, optical conductivity and nonlinear optical properties of doped ZnO-polystyrene composites films, Biointerface Res. Appl. Chem. 12 (1) (2022) 170–179.
[91] S.A. Gad, et al., ICMMS-2: enhancement of the dielectric and nonlinear optical properties of PbSe nanomaterial thin films with different contents of polyethylene glycol, Egypt. J. Chem. 64 (3) (2021) 5–6.
[92] S. Gedi, et al., Comprehensive optical studies on SnS layers synthesized by chemical bath deposition, Opt. Mater. 42 (2015) 468–475.
[93] Q. Shen, et al., Characterization of electron transfer from CdSe quantum dots to nanostructured TiO2 electrode using a near-field heterodyne transient grating technique, Thin Solid Films 516 (17) (2008) 5927–5930.